Application of poly(amidoxime)/scrap facemasks in extraction of uranium from seawater: from dangerous waste to nuclear power

Xue Zhang[1] · Bo Ouyang[2] · Guangshun Hou[3] · Pengpeng Chang[4] · Dadong Shao[1]

Abstract

To effectively kill microorganisms on scrap facemasks (FMs) surface and provide new material for extracting uranium (U(VI)) from seawater, scrap FMs was treated by N_2 capacitance coupled (CCP) plasma and modified with polyamidoxime (PAO). The obtained PAO/FMs was well characterized and applied as an adsorbent in the extraction of U(VI) from seawater. The effects of environmental conditions on the adsorption capability of PAO/FMs for U(VI) were briefly studied. Results showed that plasma technique can synchronously kill microorganisms and induce acrylonitrile (AN) polymerization on FMs surface. The prepared PAO/FMs presented excellent adsorption capability for U(VI). The experimental results highlighted the application of plasma technique in the management of scrap FMs, and PAO/FMs in the extraction of U(VI) from seawater.

Keywords Uranium · Seawater · Scrap facemasks · Plasma technique · Amidoxime

Introduction

Since the 20th century, with the continuous development of nuclear power, the demand for uranium resources has increased rapidly. The world's proven uranium resources are only 4.59 million tons, which can only support the world's existing nuclear power plants for ~60 years [1]. The ~4.5 billion tons U(VI) in seawater can sound support the world's demand for 10^4 years, which has attracted extensive attention. Various methods and materials have been applied in U(VI) recovery [2–4]. Researchers commonly believe that materials are critical for extracting U(VI) from seawater, and polyamidoxime (PAO) based adsorbents are widely used in the extraction of U(VI) from seawater due to the strong coordination between amidoxime (AO) group and U(VI) in seawater. However, due to the easy aggregation of PAO, its experimental adsorption capability is much lower than theoretical one. To improve the utilization rate of PAO in the uptake of U(VI) from seawater, PAO is usually modified onto various materials.

Coronavirus disease 2019 (COVID-19), a novel coronavirus, has killed millions of people worldwide since early 2020 [5]. The prevalence of COVID-19 deeply affects our life, such as health, economy, and life-style [6]. Like most infectious viruses, COVID-19 can be spread by droplets, which can mingle with the air quickly, and enter our body through respiration. Vaccine popularization and individual protection are effective to control methods for COVID-19, which has become continuous and regular work. To prevent the invasion of the virus, people have to wear face masks (FMs) in public. Like food, clothes, and mobile phones, now FMs have become a necessity of life [7], and the global demand for FMs is estimated to be ~129 billion per month [8]. For public-safety, FMs are usually single-use and generate a million of tons of dangerous waste in a short period [9]. Abandoned FMs have short- and long-term impacts on environment, public health, and social governance. The decomposing plastic fragments of FMs will be dispersed in nature for a long time and eventually affect environment in different

✉ Dadong Shao
  shaodadong@126.com

1   School of Environmental and Biological Engineering, Nanjing University of Science and Technology, 210094 Nanjing, P R China

2   MIIT Key Laboratory of Semiconductor Microstructure and Quantum Sensing, Nanjing University of Science and Technology, 210094 Nanjing, China

3   Institute of Resources and Environment, Henan Polytechnic University, 454000 Jiaozuo, China

4   CNNP Jiangsu Nuclear Power Co. Ltd, 222042 Lianyungang, China

forms. Seondly, large quantities of discarded FMs flows into ocean, while FMs is similar to jellyfish in shape, causing other organisms to swallow. It results in unexpectedly and seriously affecting marine ecological balance. Finally, during the epidemic, FMs worn may carry viruses. If they are discarded casually, it may lead to the second transmission of coronavirus [10]. However, the vast majority of FMs are discarded into environment around world. Therefore, proper management of scrap FMs is a global challenge.

Commercial FMs are composed of kinds of plastic or derivatives of plastic, which cannot be degraded by microorganisms [5]. Scrap FMs will come into microplastics (<5 mm), which can affect living organisms, food safety, and public health [10–12]. During the COVID-19 epidemic period, standard disinfection technologies used to treat COVID-19 medical waste include incineration, landfill, and autoclaving [13–15]. Among the above methods, incinerating is commonly used to dispose of FMs [16], which suffer from technical incompleteness in air pollution controls. The plastics in FMs melt, are volatile, and form toxic chemicals at high temperature [17–20]. To reduce environmental impacts of scrap FMs, the finding of new uses for FMs is a very urgent and esstential topic.

Pathogenic microorganisms (such as bacteria and viruses) are usually attached to small dust particles or form aerosols, which infect human beings through the respiratory tract. Filtering efficiency of medical surgical masks are $>95.0\%$ for bacteria and $>30.0\%$ for non-oily particles. Medical surgical masks can block various bacteria and viruses, and must be strict sterilized to avoid secondary contamination. Plasma contains abound high energy species (such as electron, ion, and groups), and can effectively kill microorganisms. To effectively kill microorganisms on scrap FMs surface and provide new material for extracting U(VI) from seawater, scrap FMs was treated with N_2 CCP plasma and modified with PAO. The obtained PAO/FMs was well characterized and applied as an adsorbent in extracting U(VI) from seawater. The effects of environmental conditions on the adsorption performance of PAO/FMs for U(VI) was briefly studied. The results show that the plasma technique can simultaneously kill microorganisms and induce polymerization of AN on FMs surface. The prepared PAO/FMs presents excellent adsorption capability for U(VI). Experimental results highlighted the application of plasma technique in the management of scrap FMs, and the prepared PAO/FMs in the extraction of U(VI) from seawater.

Experimental

Synthesis of PAO/FMs PAO/FMs was synthesized by plasma induced polymerization of AN on FMs surface, followed by amidoximation treatment. FMs are obtained from dedicating waste mask collection stations. Briefly, scrap FMs were treated by N_2 CCP plasma (N_2 pressure of 10 Pa and power of 10 W) in a tubular quartz reactor for 5 min at room temperature. We found that microorganisms on FMs surface cannot be observed by microscopy technique after N_2 CCP plasma treatment. The treated FMs were placed into a conical flask containing 10 mL AN, and reacted for 24 h at room temperature under N_2 and shocking conditions. After washing with ethanol, the derived PAN/FMs was amidoximated in 100 mL 66.5 g/L NH_2OH solution at 60 °C for 3 h to convert $-C\equiv N$ group into $-C(NH_2)=NOH$ group. The obtained PAO/FMs was rinsed with ethanol/water solutions and vacuum dried at room temperature.

Characterization The physiochemical properties of FMs and PAO/FMs were characterized by scanning electron microscopy (SEM), Fourier transform infrared (FT-IR) spectroscopy, Raman spectroscopy, X-ray photoelectron spectroscopy (XPS), and energy dispersive spectroscopy (EDS). The surface morphology and elemental composition were obtained using a Zeiss Supra 55 Sapphire SEM equipped with an Oxford Instrument. FT-IR spectroscopy was mounted on a Bruker Tensor II with a platinum ATR instrument at room temperature. Raman spectroscopy analysis was performed by Raman spectrometry (LabRam HR). XPS spectroscopy was performed by an ESCALab220i- XL surface microanalysis system (VG Scientific) equipped with an Al Kα (hλ = 1486.6 Ev) source at a chamber pressure of 3×10^{-9} mbar. The surface charging effects were corrected with the carbon 1s photoelectron spectra (C 1s) at 284.4 eV as a reference.

Application of PAO/FMs in the extraction of U(VI) from seawater The application of PAO/FMs in U(VI) extraction from seawater was studied by batch method, and the PAO/FMs was cut into small uniform pieces, weighing 0.0200 g. Different concentrations of U(VI) solutions were prepared by dissolving $UO_2(NO_3)_2\cdot6H_2O$ ($>9\%$ purity, purchased from meryer) in deionized water. PAO/FMs and NaCl were pre-equilibrated for 24 h to achieve electrolyte balance, and then U(VI) solution and deionized water were added to achieve the desired compositions. The U(VI) containing solution was prepared with different concentrations, and the total volume was 50 mL. NaOH or HCl was used to adjust solution pH. After shaking for desired time, the suspension was filtered with a 0.45 μm needle filter for subsequent testing. The final U(VI) concentrations of mg/L and μg/L levels in supernatants were measured on an Optima 2100 DV inductively coupled plasma atomic emission spectroscopy (ICP-AES, Perkin Elmer) and ICP-mass spectroscopy (ICP-MS, Thermo Scientific X-Series II), respectively. The

instrumentation and operating parameters of ICP-MS are detailed in Table S1.

Results and discussion Characterization of FMs and PAO/FMs SEM and EDS techniques were used to study the morphology of FMs and PAO/FMs. As shown in Figure S1, the lower magnification factor microscopy images of FMs and PAO/FMs at 40x, 100x, and 200x reveal the internal fiber morphology. From the 40x microscopy images, the morphology of FMs is intact throughout the process. Gelatinous can be found on FMs layer of 100x and 200x magnification factor of the SEM image, which is formed during the spraying and melting process. Further magnification factor of SEM image the is shown in Fig. 1. SEM image magnification was divided into three groups: 1000x, 2000x, and 10000x (Fig. 1 A-1I). The three groups' SEM images

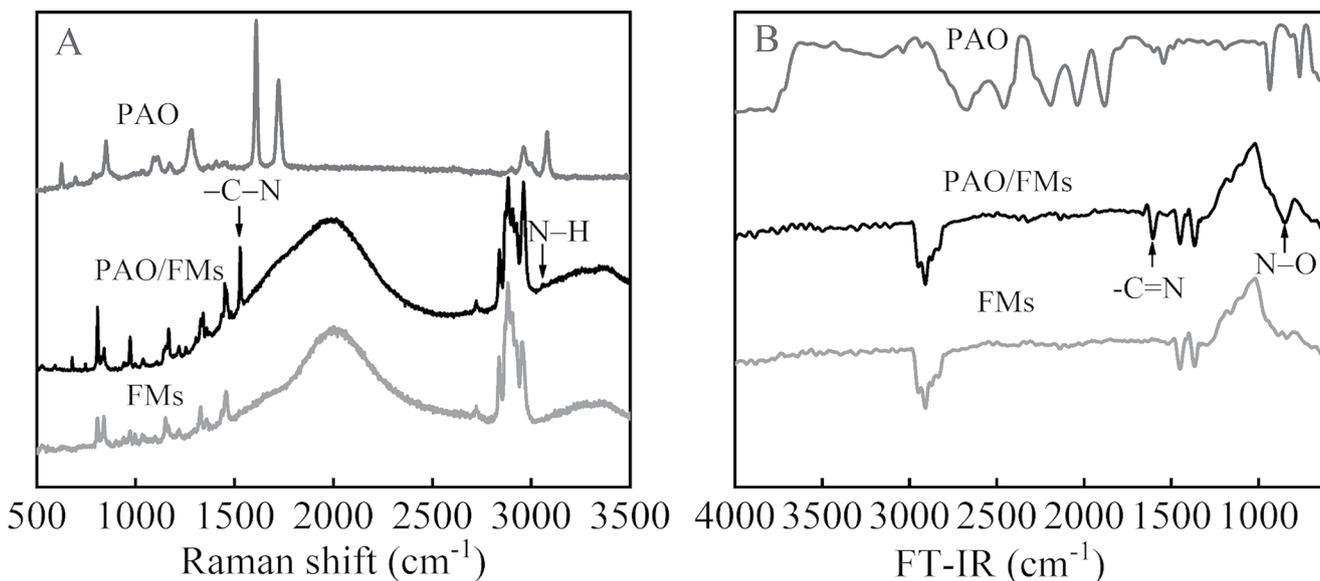**Fig. 1** SEM images of FMs (A-C), PAO/FMs (D-F) and U(VI)-laden PAO/FMs (G-I)
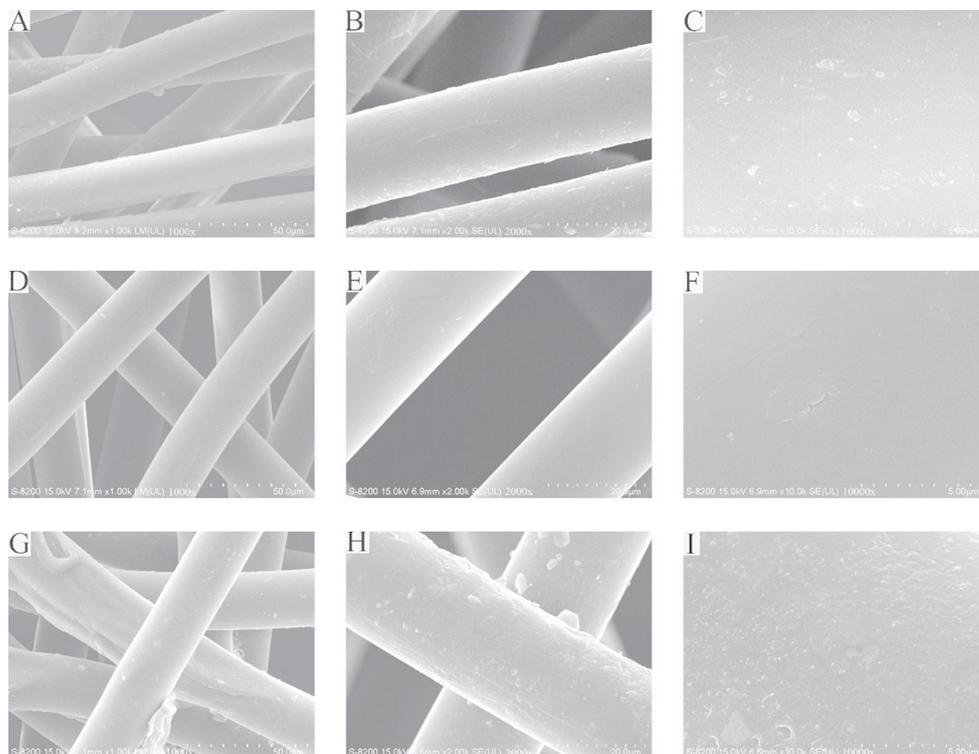

Fig. 2 Raman spectra (A) and FT-IR spectra (B) of PAO/FMs and FMs

show the surface morphology and fiber changes. PAO/FMs (Fig. 1D F) showed similar surface morphology to FMs (Fig. 1 A-1 C) and became cleaner, filled, and covered with a thin layer. It reveals that N_2 CCP plasma treatment, AN polymerization, and amidoximation treatment did not destroy the morphology of FMs, and the modified PAO formed a thin film on PAO/FMs surface. The U(VI)-laden PAO/FMs is rough and bigger (Fig. 1G and I), which can be assigned to the penetration of H_2O into PAO/FMs polymeric structure. We also found similar results of phosphate fuctionalized polyethylene [21]. The EDS technique (Figure S2) was used to explore the element distribution on the U(VI)-laden PAO/FMs surface. PAO/FMs surface was almost uniformly covered by U(VI) and PAO, revealing PAO's uniform distribution on PAO/FMs surface.

Raman spectroscopy has unique advantages in characterizing the degree of surface disorder of carbon-based materials, and is a simple and effective method to study FMs and PAO/FMs surface functionalization. The disorder degree of FMs, and PAO/FMs can be well studied by Raman technique, and the results are depicted in Fig. 2 A. FMs, PAO, and PAO/FMs show typical Raman peaks in three regions: the peak at 2800–3000 cm^{-1} relates to the stretching vibration of C-H bond; the peak at 800–1500 cm^{-1} is related to the stretching vibration of C-C bond, and the bending vibration of C-H bond; the peak at 200–550 cm^{-1} is the fingerprint region of polypropylene fiber which caused by the wobbling vibration from a carbon chain skeleton. Notably, the peak at ~ 2800 cm^{-1} is "red shift" caused by the modified PAO on PAO/FMs surface. The Raman peak of PAO/FMs at ~ 3363 cm^{-1} can be assigned to the stretching vibration of the N-H bond.

FT-IR spectra of PAO, PAO/FMs, and FMs were detected and compared in Fig. 2B. Two characteristic peaks (1654 and 939 cm^{-1} of C=N and −N−O, respectively) relate to the amidoxime group of PAO can be dound in the spectrum of PAO. After amidoximation treatment, the absorption
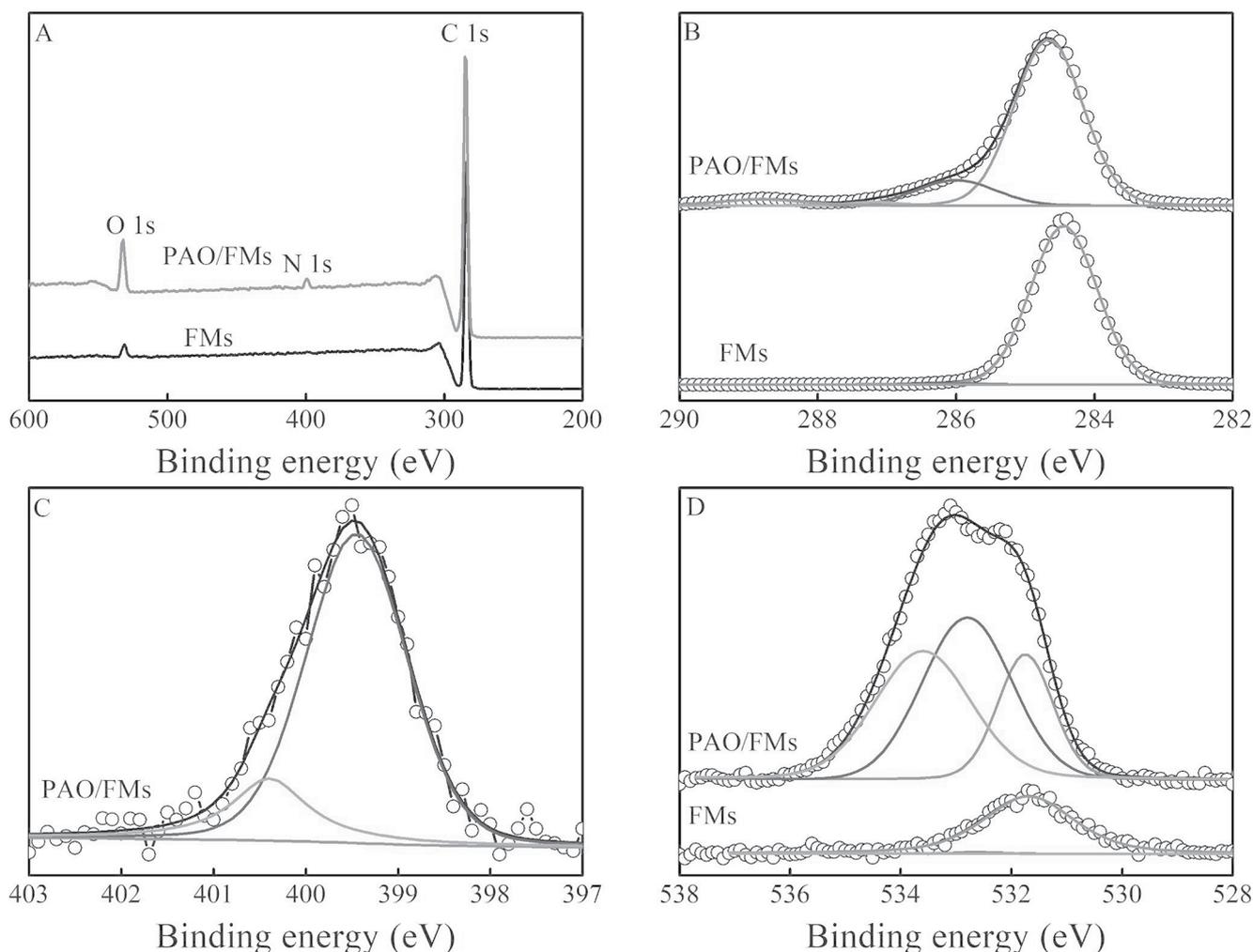

Fig. 3 XPS survey (A), C 1s (B), N 1s (C), and O 1s (D) spectra of FMs and PAO/FMs

peaks at 2836–2949 cm^{-1} belong to the antisymmetric and symmetric stretching vibration peaks of C-H in fiber backbone -CH$_2$-CH-. New peaks of PAO/FMs related to C=N and N-O [22, 23] at 1648 cm^{-1} and 911 cm^{-1} indicate that PAO was successfully modified on the FMs surface.

We provided information on the chemical composition of PAO/FMs and FMs by XPS technique and further analyzed

Table 1 Curve fitting results of XPS C 1s spectrum

	Peak	BE[a] (eV)	FWHM[b] (eV)	%
FMs	C-C	284.44	1.13	99.4
	C–OH	286.05	1.00	0.65
	–C=O	287.50	1.00	0.00
	–COOH	288.70	1.00	0.00
PAO/FMs	C-C	284.66	1.17	80.9
	C–OH, –C(NH$_2$)=NOH	286.00	1.34	14.0
	–C=O	287.16	0.85	1.17
	–COOH	288.80	1.45	3.98

a: Binding energy; b: Full width at half-maximum

Table 2 Curve fitting results of XPS N 1s spectrum

	Peak	BE (eV)	FWHM (eV)	%
PAO/FMs	-C≡N	398.80	1.00	0.01
	N-H	399.45	1.29	82.7
	–C(NH$_2$)=NOH	400.40	0.98	17.3

Table 3 Curve fitting results of XPS O 1s spectra

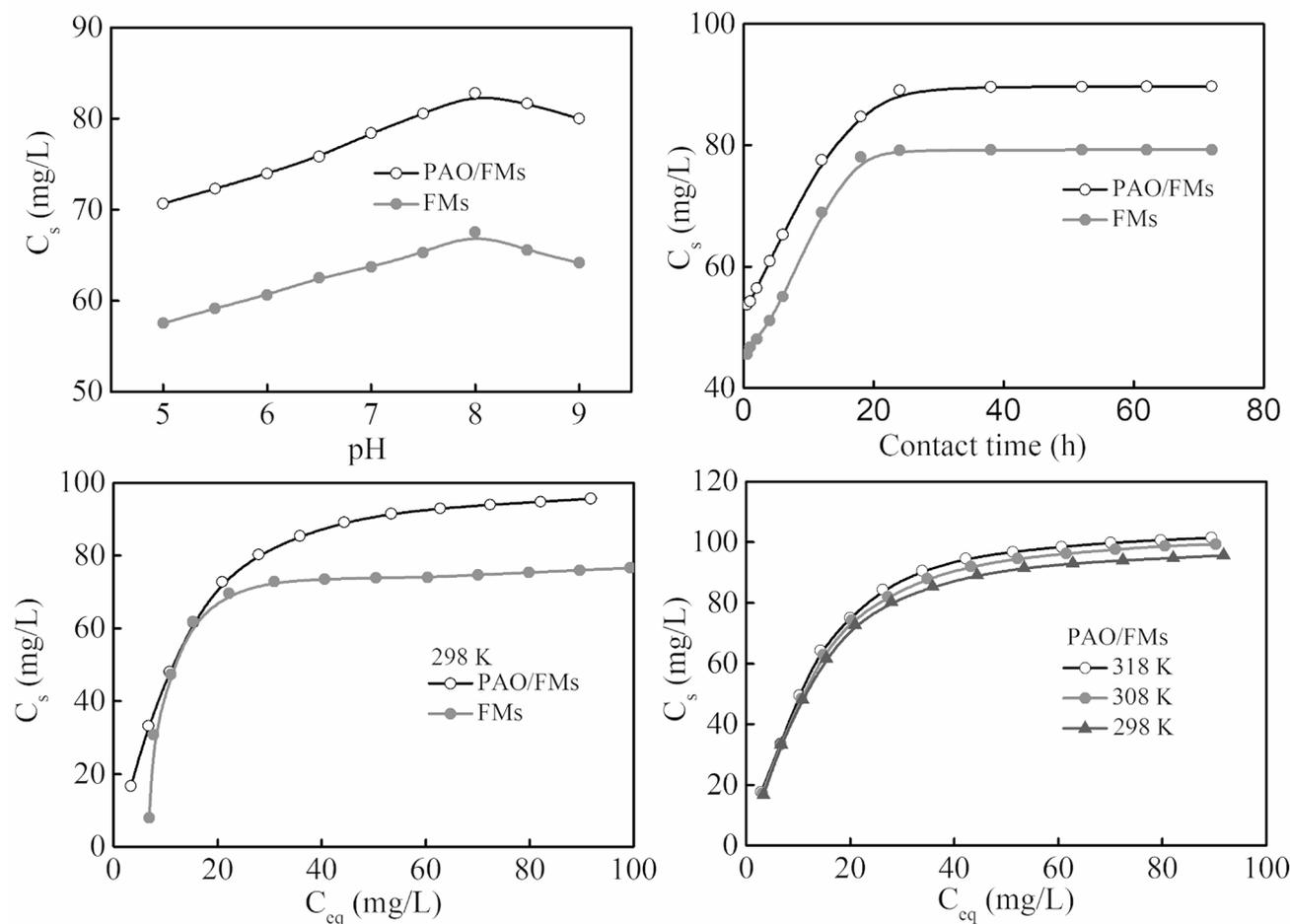|	Peak	BE (eV)	FWHM (eV)	%
FMs	-COOH	531.68	1.92	99.1
	C=O	532.60	1.00	0.90
	-OH	533.66	1.00	0.00
PAO/FMs	-COOH	531.75	1.18	20.8
	C=O, –C(NH$_2$)=NOH	532.80	1.90	41.7
	-OH	533.60	2.04	37.5

Fig. 4 Effect of pH (A), contact time (B), adsorption isotherms (C), and reaction temperature (D) on the adsorption of U(VI) on FMs and on PAO/FMs from solution. m/V=0.40 g/L, I=0.1 mol/L NaCl. Figure 4 A: T=298±1 K, contact time: 24 h, C[U(VI)]$_{initial}$ = 50.0 mg/L. Figure 4B: T=298±1 K, pH=8.2±0.1, C[U(VI)]$_{initial}$= 50.0 mg/L. Figure 4 C: T=298±1 K, pH=8.2±0.1, contact time: 24 h. Figure 4D: pH=8.2±0.1, contact time: 24 h

the existing form of NH-C=N-OH groups on PAO/FMs surface. The XPS survey spectra of FMs and PAO/FMs (Fig. 3 A) showed the characteristic oxygen 1s photoelectron spectra (O 1s), nitrogen 1s photoelectron spectra (N 1s), and C 1s peaks at 532 eV, 399 eV, and 284 eV, respectively. The relative peak intensity and signal-to-noise ratio of the XPS O 1s spectrum of PAO/FMs are sound increase, which indicates that PAO/FMs have more oxygen-containing species than FMs.

The XPS spectra of C 1s (Fig. 3B) on the surface of PAO/FMs was divided into four components of C–C, C–OH, and –$C(NH_2)$=NOH, –C=O, and –COOH, which were at 284.5 ± 0.2, 286.0 ± 0.2, 287.3 ± 0.2, and 288.8 ± 0.1 eV, respectively. According XPS C 1s spectra (Table 1), C-C was the dominant carbon species on FMs surface. Due to the modification of PAO, the peak fractions of C-OH and –$C(NH_2)$=NOH are increased.

XPS N 1s spectrum of PAO/FMs (Fig. 3 C) was divided into three peaks. The peaks at 398.80, 399.45, and 400.40 eV were consistent with –C≡N, undoped amine-like N atoms (N–H), and –$C(NH_2)$=NOH, respectively [24]. According to the fitting results of N 1s XPS spectrum (Table 2), the peak fraction corresponding to –C≡N was neglectable, and N–H and –$C(NH_2)$=NOH were the dominant N species on PAO/FMs surface. It reveals the excellent conversion of PAN to PAO in the amidoximation process.

XPS O 1s spectrum (Fig. 3D) could be divided into –COOH, C=O and –$C(NH_2)$=NOH, and –OH, which were centered at 531.7 ± 0.2, 532.7 ± 0.2, and 533.6 ± 0.2 eV, respectively. According to the fitting results of XPS O 1s spectra (Table 3), the O atoms on FMs surface almost existed as -COOH, C=O; –$C(NH_2)$=NOH-OH are the dominant oxygen species on PAO/FMs surface, which is consistent with the results of XPS C 1s and N 1s spectra. Adsorption performance of PAO/FMs At different pH values and CO_2 partial pressures, U(VI) tends to form various U(VI)-hydroxide and Ca/Mg-U(VI)-carbonate ternary species, and the uptake of U(VI) from seawater is mainly limited by the decomposition of Ca/Mg-U(VI)-carbonate ternary species to free UO_2^{2+}. The carbonate concentration fairly depends on the partial pressure of CO_2 in atmosphere. The partial pressure of CO_2 is measured to be 38–40 Pa under our experimental condition. U(VI) mainly exists as positively charged U(VI) species at pH < 4 [25–32]. Meanwhile, the adsorbent surface gradually changes from positive charge to negative charge with increasing solution pH in the low

ranges. The increased negative surface charges attract more positively charged U(VI) species and consequently increase their adsorption capacity in acidic solutions. In a highly basic solution, U(VI) mainly exists as negatively charged U(VI) species, and the adsorbent surface is negatively charged. Due to electrical repulsion, it is difficult for a negatively charged surface to adsorb negatively charged U(VI) species in a strongly basic solution. To explore the impact of pH, the pH effect on the adsorption performance was studied at pH 5–9 (Fig. 4 A). We found that the maximum adsorption capability for FMs and PAO/FMs is at pH ~ 8.

If the adsorption of U(VI) ions in seawater on adsorbent surface can quickly completed under marine conditions, the required operation time for complete U(VI) extraction will be significantly shortened, which will solve the problem of long-term immersion of adsorbent in seawater. To explore the required runtime of FMs and PAO/FMs in potential applications, the adsorption kinetics of FMs and PAO/FMs were obtained at 298 K, and the results are shown in Fig. 4B. The adsorption capacity of U(VI) on FMs and PAO/FMs surfaces increased with the prolongation of reaction time after 20 h and remained unchanged thereafter. The adsorption kinetics were analyzed by pseudo first order ($q_t = q_e \times (1 - \exp(-k_1 \times t))$, where q_e and q_t (mg/g) are the adsorbed amounts of U(VI) at equilibrium time and time t (h), respectively, and $k_1 t$ (1/h) is pseudo first order kinetic constant) and pseudo second order ($q_t = q_e \times t/(1/(K' \times q_e) + t)$, where K' (g/(mg·h)) is pseudo second order kinetic constant) models. The parameters of the pseudo-first-order and pseudo-second-order kinetic models are shown in Figure S3 and Table 4. From the relevant parameters (R^2), it can be seen that the adsorption process of PAO/FMs to U(VI) conforms to the pseudo-second-order adsorption model. It reveals that chemical adsorption is the main adsorption method in the process of FMs and on PAO/FMs adsorption of U(VI).

The adsorption capacity of adsorbent can be widely evaluated by adsorption isotherms. In this work, the effect of modified PAO on the adsorption capacity of PAO/FMs for U(VI) was studied. As shown in Fig. 4 C, the adsorption isotherms of U(VI) on PAO/FMs are much higher than that on FMs under same experimental conditions (pH 8.2 ± 0.1 and 298 ± 1 K). This reveals that the modified PAO on PAO/FMs surface can significantly enhance the adsorption capacity of PAO/FMs for U(VI). Langmuir ($C_s = b \times C_{s,max} \times C_{eq}/(1 + b \times C_{eq})$, where C_{eq} is the equilibrium

Table 4 Parameters for kinetic models of U(VI) adsorption on FMs and on PAO/FMs at pH 8.2 ± 0.1, T = 298 ± 1 K

	Pseudo-first-order			Pseudo-second-order		
	q_e (mg/g)	k_1 (mg/(g·h))	R^2	q_e (mg/g)	K' (g/(mg·h))	R^2
FMs	71.7	1.04	0.407	76.5	0.0176	0.698
PAO/FMs	80.7	1.24	0.400	85.8	0.0190	0.702

concentration of U(VI) after adsorption, $C_{s,max}$ (mg/g), and b (L/mg) are the maximum adsorption capability of adsorbent and the Langmuir constant, respectively) and Freundlich ($C_s = K \times C_e^{1/n}$, K (mg/g) and 1/n are the constant indicative of the adsorption capability and intensity, respectively) models were used to fitting the experimental data, and the mechanism of adsorption process was discussed. The relevant adsorption isotherm parameters can be calculated from the fitting curves of the two models, as shown in Table 5. Langmuir and Freundlich isotherm linear fitting parameters were compared, and the Langmuir isotherm model could better fit the adsorption process, indicating that the adsorption of U(VI) on PAO/FMs surface is a single-layer chemisorption.

The effect of reaction temperature on U(VI) adsorption performance was studied at three different temperatures (i.e., 298, 308, and 318 K), and the results are shown in Fig. 4D. The adsorption isotherms of U(VI) on PAO/FMs surface gradually increased when the reaction temperature increased from 298 to 318 K. The related thermodynamic parameters of U(VI) adsorption on PAO/FMs surface, including standard enthalpy change ($\Delta H°$), standard Gibbs free energy ($\Delta G°$), and entropy change ($\Delta S°$) were calculated and shown in Table 6. The positive value of $\Delta H°$ indicates that PAO/FMs surface adsorption on U(VI) ion is an endothermic process, and the increase of temperature is conducive to the adsorption, which is consistent with the improvement of U(VI) adsorption at higher reaction temperatures. The value of $\Delta G°$ is negative, indicating that the adsorption process of PAO/FMs to U(VI) is spontaneous at different temperatures. The value of $\Delta S°$ is positive, indicating PAO/FMs surface and solution disorder increase during the adsorption process.

Seawater is a very complex matrix, and the presence of numerous of metal ions will negatively affect the adsorption of U(VI) ions. Na(I), K(I), Ca(II), and Mg(II) is the predominant cations in seawater. The distribution coefficient (K_d) is the ratio of the radionuclide concentration adsorbed by solid (C_s) and the concentration in liquid (C_e), given by $K_d = C_s/C_e$. K_d is an empirical parameter defined as the ratio of the quantity of contaminant adsorbed per solid mass (geological deposit) to the quantity of contaminant remaining in per aqueous phase (ground water) at chemical equilibrium (or at "quasi-equilibrium" state reached during the experiment). Inherent in the K_d model (or "linear isotherm" adsorption

Table 6 Thermodynamic parameters of U(VI) adsorption on PAO/FMs surface

T (K)	lnK_d	Thermodynamic parameters		
		ΔG^0 (kJ/mol)	ΔH^0 (kJ/mol)	ΔS^0 (J/(mol·K))
298	8.69	-21.5	3.48	83.8
308	8.69	-22.2		
318	8.78	-23.2		

model) is the assumption that the adsorption of contaminant on solid phase is linearly dependent on its concentration in aqueous phase. This assumption typically holds only for low contaminant concentrations in solution [33]. According to the data shown in Fig. 5 A that the adsorption of U(VI) on PAO/FMs showed a downward trend with increasing ionic strength, the adsorption U(VI) ion amount in the four cation solutions was K(I) > Na(I) > Mg(II) > Ca(II) under the same experimental conditions. This is mainly because the formation of Ca/Mg-CO_3^{2-}-UO_2^{2+} complexes has a significant negative effect on U(VI) adsorption [34, 35]. Endrizzi et al. [27] and Baghdadi et al. [36] reported that these ternary complexes determined U(VI) behavior in seawater and were hard to be adsorbed. Based on the fact that heavymetal ions (such as Cu(II), Al(III), Fe(III), and V(IV)) can compete with U(VI) for adsorption sites, and thus significantly decrease the extraction of U(VI) from seawater [37, 38]. The adsorption capacities of PAO/FMs for U(VI) and those heavy metal ions were also studied, respectively. The results in Fig. 5B show that the PAO/FMs selectively adsorb U(VI) in the presence of those heavy-metal ions very well under the same experimental conditions. This reveals the high selectivity of PAO/FMs toward U(VI) compared with heavy-metal ions in seawater.

The regeneration and reusability of PAO/FMs are significant for practical application. To further investigate its regeneration performance, the PAO/FMs after U(VI) adsorption was eluted to recover the U(VI) and regenerate the adsorbents. In this work, to avoid the degradation of the PAO-based materials caused by the acid solution, the alkaline solution Na_2CO_3 was used to elute the agent. Desorption efficiency vs. the concentration of Na_2CO_3 was indicated in Fig. 6 A, as the Na_2CO_3 concentration increased from 0.002 mol/L to 0.1 mol/L, the desorption amount of U(VI) from PAO/FMs surface quickly. The results clearly illustrate that 0.1 mol/L Na_2CO_3 was sufficient for the quantitative desorption of U(VI) ions from the surfaces of PAO/FMs.

Table 5 Parameters calculated from Langmuir and Freundlich models for U(VI) adsorption on FMs and on PAO/FMs at pH 8.2 ± 0.1

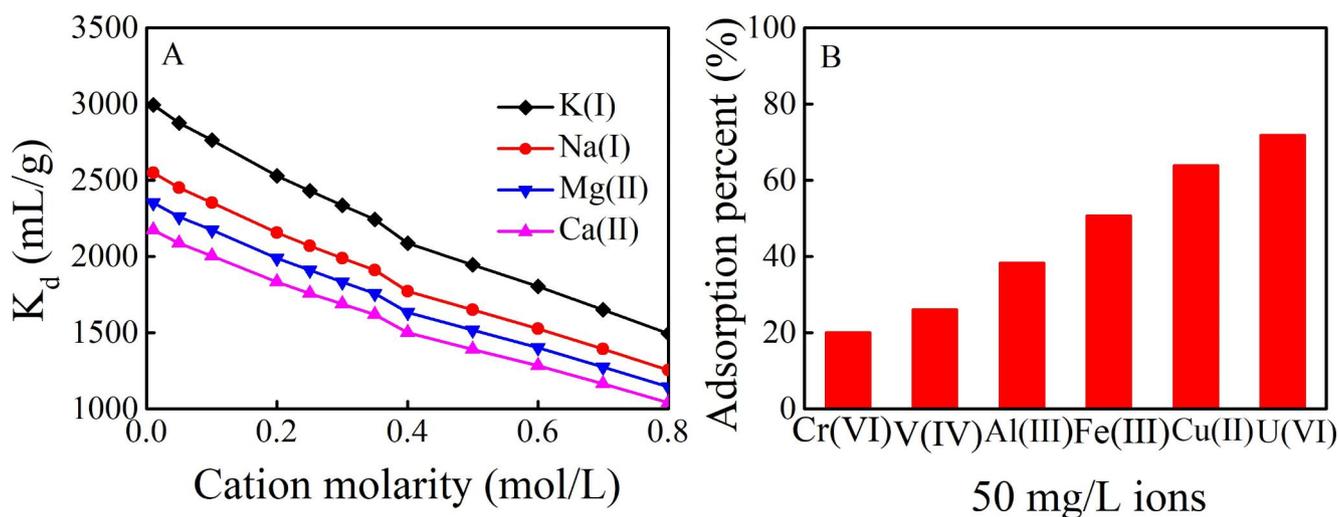|	T (K)	Langmuir model			Freundlich model		
		$C_{s,max}$ (mg/g)	b (L/mg)	R^2	K (mg/g)	1/n	R^2
FMs	298	91.0	0.0728	0.961	18.2	0.336	0.837
PAO/FMs	298	114	0.0733	0.985	22.4	0.343	0.889
	308	119	0.0716	0.987	22.6	0.350	0.897
	318	121	0.0743	0.985	23.7	0.346	0.893

Fig. 5 Effect of cation on U(VI) distribution coefficient (K_d) on PAO/FMs surface (A). Comparison enrichment performance of 50.0 mg/L U(VI) and heavy metal ions on PAO/FMs surface (B). T = 298 ± 1 K, contact time: 24 h, m/V = 0.40 g/L, pH = 8.2 ± 0.1. Figure 5 A: C[U(VI)]$_{initial}$ = 50.0 mg/L. Figure 5B: I = 0.1 mol/L NaCl

Thus, 0.1 mol/L Na_2CO_3 solutions was chosen as the eluent the adsorbent. As shown in Fig. 6 B, although the adsorption and elution rates of PAO/FMs exhibited minor changes during the multiple cycles, the PAO/FMs still showed excellent reusability performance in extraction U(VI) from seawater after eight-time cycles. Real application of PAO/FMs Based on the excellent adsorption capability of PAO/FMs for U(VI), the real application of PAO/FMs in the extraction of U(VI) from environmental solutions was studied. We first evaluated the performance of PAO/FMs in diluted U(VI) solution (mass to volume ratio (m/V) = 0.40 g/L, pH 8.2). As shown in Table 7, PAO/FMs can quantitatively uptake mg/L levels U(VI). We then evaluated the performance of PAO/FMs in the extraction of U(VI) from running water,

and μg/L level U(VI) was intentionally added. PAO/FMs can still sound extract μg/L level U(VI) from this complex system. Therefore, the real application of PAO/FMs in extraction U(VI) from seawater was performed, and the seawater was prepared with sea salt. The high salt matrix of seawater will precipitate in the cone mouth of ICP-MS after long-term injection, making the sampling cone and skimmer cones smaller, reducing the injection volume, and affecting the stability of analysis [39]. Thus, 0.05 mol/L HNO_3 was used to dilute seawater to reduce the high salt matrix's separate. We found that PAO/FMs can effectively uptake ~ 39% of 3.8 μg/L U(VI) from seawater. Experimental results confirm the high efficiency of PAO/FMs in the extraction of U(VI) from seawater.
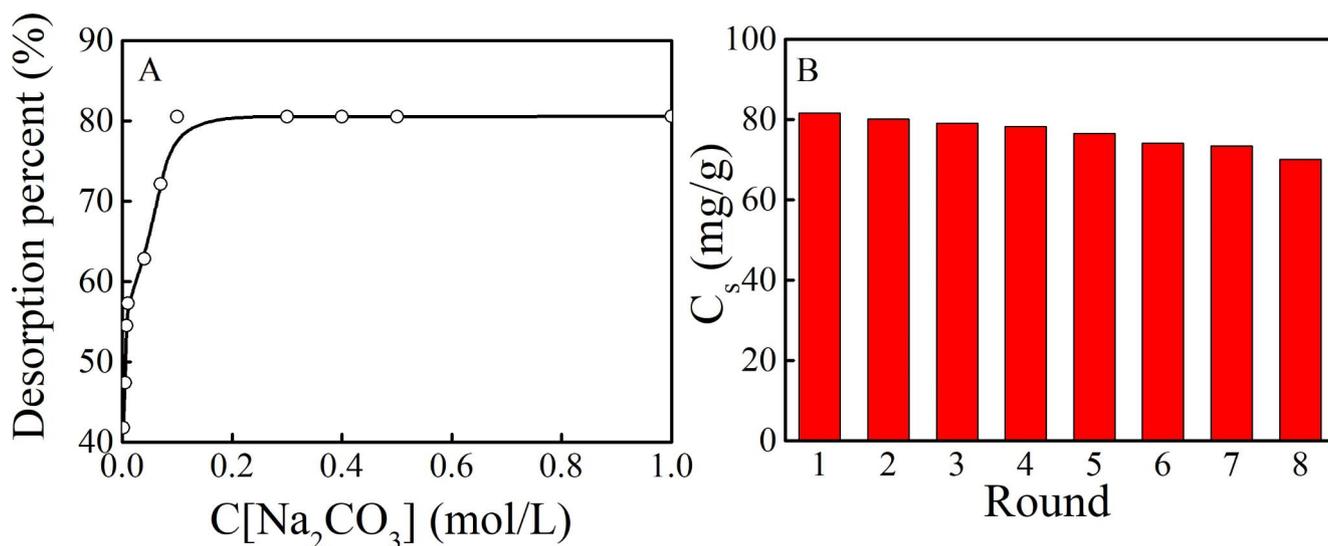

Fig. 6 Effect of Na_2CO_3 concentration on the desorption of U(VI) from PAO/FMs (A). Recycling time on the adsorption capability of PAO/FMs for U(VI) (B). Figure 6B: T = 298 ± 1 K, contact time: 24 h, m/V = 0.40 g/L, C[U(VI)]$_{initial}$ = 50.0 mg/L, pH = 8.2 ± 0.1, I = 0.1 mol/L NaCl

Table 7 Selected results of U(VI) adsorption on PAO/FMs surface at m/V = 0.40 g/L, T = 298 ± 1 K, contact time: 24 h, pH 8.2 ± 0.1

Sample	C[U(VI)] (ug/L)		Adsorption (%)
	Initial	Final	
Diluted U(VI) sloution	50,000	17,400	65.2
	20,000	2580	87.1
	10,000	880	91.2
	1000	107	89.3
Running water	1000	204	79.6
	100	31.8	68.2
	10	4.27	57.3
Seawater	100	38.9	61.1
	10	5.32	46.8
	3.8	2.33	38.7

Conclusions

In summary, plasma technology can well achieve the proper management of huge scrap FMs under the global epidemic of coronavirus COVID-19. PAO/FMs was synthesized for the first time as an effective adsorbent for adsorption U(VI) and can be used as a candidate for extracting U(VI) from seawater. The experimental results highlight the application of plasma technique in the management of huge scrap FMs and the application of treated scrap FMs in the extraction of U(VI) from seawater.

Declarations

Conflict of interest The authors declare that they have no conflict of interest.

References

1. Anirudhan TS, Lekshmi GS, Shainy F (2019) Synthesis and characterization of amidoxime modified chitosan/bentonite composite for the adsorptive removal and recovery of uranium from seawater. J Colloid Interf Sci 534:248–261

2. Yue Y, Mayes RT, Kim J et al (2013) Seawater uranium sorbents: preparation from a mesoporous copolymer initiator by atom transfer radical polymerization. Angew Chem Int Ed 52:13458–13462

3. Bai Z, Wang Y, Li Y et al (2016) First cationic uranyl organic framework with anion-exchange capabilities. Inorg Chem 55:6358–6360

4. Liu C, Hsu PC, Xie J et al (2017) A half-wave rectified alternating current electrochemical method for uranium extraction from seawater. Nat Energy 2:17007

5. Behera BC (2021) Challenges in handling COVID-19 waste and its management mechanism: a review. Environ Nanotechnol Monit Manag 15:100432

6. Costa JP (2021) The 2019 global pandemic and plastic pollution prevention measures: Playing catch-up. Sci Total Environ 774:145806

7. Yousef S, Eimontas J, Striugas N et al (2021) Pyrolysis kinetic behaviour and TG-FTIR-GC-MS analysis of coronavirus face masks. J Anal Appl Pyrol 156:105118

8. Saberian M, Li J, Kilmartin-Lynch S et al (2021) Repurposing of COVID-19 single-use face masks for pavements base/subbase. Sci Total Environ 769:145527

9. Botetzagias I, Malesios C (2021) Do single-use facemask users' care for the effects on the (marine) environment during the COVID-19 pandemic? Preliminary results from Greece. Mar Pollut Bull 167:112320

10. De-la-Torre GE, Rakib MRJ, Pizarro-Ortega CI et al (2021) Occurrence of personal protective equipment (PPE) associated with the COVID-19 pandemic along the coast of Lima. Peru Sci Total Environ 774:145774

11. Silva ALP, Prata JC, Walker TR et al (2020) Rethinking and optimizing plastic waste management under COVID-19 pandemic: Policy solutions based on redesign and reduction of single-use plastics and personal protective equipment. Sci Total Environ 742:140565

12. Chowdhury H, Chowdhury T, Sait SM (2021) Estimating marine plastic pollution from COVID-19 face masks in coastal regions. Mar Pollut Bull 168:112419

13. Singh N, Tang Y, Ogunseitan OA (2020) Environmentally sustainable management of used personal protective equipment. Environ Sci Technol 54:8500–8502

14. Jung S, Lee S, Dou X et al (2021) Valorization of disposable COVID-19 mask through the thermo-chemical process. Chem Eng J 405:126658

15. Hantoko D, Li X, Pariatamby A et al (2021) Challenges and practices on waste management and disposal during COVID-19 pandemic. J Environ Manage 286:112140

16. Geyer R, Jambeck JR, Law KL (2017) Production, use, and fate of all plastics ever made. Sci Adv 3:e1700782

17. Wang X, Ma D, Jin Q et al (2019) Synergistic effects of biomass and polyurethane co-pyrolysis on the yield, reactivity, and heating value of biochar at high temperatures. Fuel Process Technol 194:106127

18. Zhao H, Wang J (2018) Chemical-looping combustion of plastic wastes for in situ in-hibition of dioxins. Combust Flame 191:9–18

19. Su G, Ong HC, Ibrahim S et al (2021) Valorisation of medical waste through pyrolysis for a cleaner environment: progress and challenges. Environ Pollut 279:116934

20. Selvaranjan K, Navaratnam S, Rajeevc P et al (2021) Environmental challenges induced by extensive use of face masks during COVID-19: A review and potential solutions. Environ Chall 3:100039

21. Shao D, Li Y, Wang X et al (2017) Phosphate-functionalized polyethylene with high adsorption of uranium(VI). ACS Omega 2:3267–3275

22. Li S, Wei D, Guan Y et al (2014) Preparation and characterization of a permanently antimicrobial polymeric material by covalent bonding. Eur Polym J 51:120–129

23. Wei DF, Zhou RH, Zhang YW et al (2013) Acrylonitrile copolymers containing guanidine oligomer: synthesis and use for the preparation of nonleaching antimicrobial acrylic fibers. J Appl Polym Sci 130:419–425

24. Shao D, Hou G, Chi F et al (2021) Transformation details of poly(acrylonitrile) to poly(amidoxime) during the amidoximation process. RSC Adv 11:1909–1915

25. Endrizzi F, Rao L (2014) Chemical speciation of uranium (VI) in marine environments: complexation of calcium and magnesium ions with $[(UO_2)(CO_3)_3]^{4-}$ and the effect on the extraction of uranium from seawater. J Chem Eur 20:14499–14506

26. Leggett CJ, Rao L (2015) Complexation of calcium and magnesium with glutarimidedioxime: implications for the extraction of uranium from seawater. Polyhedron 95:54–59

27. Endrizzi F, Leggett CJ, Rao L (2016) Scientific basis for efficient extraction of uranium from seawater. I: understanding the

chemical speciation of uranium under seawater conditions. Ind Eng Chem Res 55:4249–4256

28. Tian G, Teat SJ, Rao L (2013) Thermodynamic studies of U(VI) complexation with glutardiamidoxime for sequestration of uranium from seawater. Dalton Trans 42:5690–5696

29. Li B, Wang L, Li Y et al (2017) Conversion of supramolecular organic framework to uranyl-organic coordination complex: a new "matrix-free" strategy for highly efficient capture of uranium. RSC Adv 7:8985–8993

30. Zhang L, Su J, Yang S et al (2015) Extended X-ray absorption fine structure and density functional theory studies on the complexation mechanism of amidoxime ligand to uranyl carbonate. Ind Eng Chem Res 55:4224–4230

31. Zhu J, Liu Q, Li Z et al (2017) Recovery of uranium (VI) from aqueous solutions using a modified honeycomb-like porous carbon material. Dalton Trans 46:420–429

32. Liu Q, Zhu J, Tan L et al (2016) Polypyrrole/cobalt ferrite/multi-walled carbon nanotubes as an adsorbent for removing uranium ions from aqueous solutions. Dalton Trans 45:9166–9173

33. Timothy E, Brendler V, Josick M et al (2011) Assessment of surface area normalisation for interpreting distribution coefficients (K_d) for uranium sorption. J Environ Radioact 102:888–895

34. Mehio N, Williamson B, Oyola Y et al (2016) Acidity of the poly (acrylamidoxime) adsorbent in aqueous solution: determination of the proton affinity distribution via potentiometric titrations. Ind Eng Chem Res 55:4217–4223

35. Tsantis ST, Zagoraiou E, Savvidou A et al (2016) Binding of oxime group to uranyl ion. Dalton Trans 45:9307–9319

36. Bghdadi S, Bouvier-Capely C, Ritt A et al (2015) Impact of the uranium(VI) speciation in mineralized urines on its extraction by calix6 arene bearing hydroxamic groups used in chromatography columns. Talanta 144:875–882

37. Pan HB, Kuo LJ, Wai CM et al (2016) Elution of uranium and transition metals from amidoxime-based polymer adsorbents for sequestering uranium from seawater. Ind Eng Chem Res 55:4313–4320

38. Mehio N, Ivanov AS, Ladshaw AP et al (2016) Theoretical study of oxovanadium (IV) complexation with formamidoxime: implications for the design of uranyl-selective adsorbents. Ind Eng Chem Res 55:4231–4240

39. Olga V, Andrei R (2021) Direct seawater analysis by high-resolution ICP-MS provides insights into toxic metal accumulation in marine sediments. At Spect 42:85–90

Publisher's note Springer Nature remains neutral with regard to jurisdictional claims in published maps and institutional affiliations.